J. Hydrol. Hydromech., 72, 2024, 4, 499–512
https://doi.org/10.2478/johh-2024-0025

sciendo Journal of Hydrology and Hydromechanics Institute of Hydrology SAS

Applying a time-varying GEV distribution to correct bias in rainfall quantiles derived from regional climate models

Milan Onderka[1,2*], Jozef Pecho[1,4], Ján Szolgay[3], Silvia Kohnová[3], Marcel Garaj[1], Katarína Mikulová[1], Svetlana Varšová[2], Veronika Lukasová[2], Roman Výleta[3], Agnieszka Rutkowska[5]

[1] Slovak Hydrometeorological Institute, Jeséniova 17, 833 15 Bratislava, Slovakia.
[2] Earth Science Institute, Slovak Academy of Sciences, Dúbravská cesta 9, 840 05, Bratislava, Slovakia.
[3] Department of Land and Water Resources Management, Faculty of Civil Engineering, Slovak University of Technology in Bratislava, Radlinského 11, 810 05 Bratislava, Slovakia.
[4] Department of Astronomy, Physics of the Earth and Meteorology, Faculty of Mathematics, Physics and Informatics, Comenius University in Bratislava, Mlynská dolina F2, 842 48 Bratislava, Slovakia.
[5] Department of Applied Mathematics, Faculty of Environmental Engineering and Land Surveying, University of Agriculture in Kraków, Balicka 253C, Kraków, Poland.
[*] Corresponding author. E-mail: milan.onderka@shmu.sk

Abstract: Climate warming is causing an increase in extreme hydrometeorological events in most parts of the world. This phenomenon is expected to continue and will affect the frequency and intensity of extreme precipitation events. Although bias correction in regional climate model simulations has also been used to assess changes in precipitation extremes at daily and longer time steps, trends in the series predicted have seldom been considered. We present a novel bias correction technique that allows for the correcting of biases in the upper tails of the Generalized Extreme Value (GEV) distribution, while preserving the trend in projected precipitation extremes. The concept of non-stationary bias correction is demonstrated in a case study in which we used four EURO-CORDEX RCM models to estimate future rainfall quantiles. Historical observations have been used to correct biases in historical runs of the RCMs. The mean relative change in rainfall quantiles between the 1991–2021 historical period and the time horizon of 2080 was found to be 13.5% (st. dev.: 2.9%) for the return period of 2 years, which tends to decline with increasing return periods. Upon the return periods of 50 and 100 years, the mean relative change was predicted to be 5.5% (st. dev.: 1.1%) and 4.8% (st. dev.: 1%), respectively.

Keywords: Non-stationarity; Climate change; Trends; Bias correction; GEV distribution.

1 INTRODUCTION

Intensive short-term rainfall can potentially lead to floods, particularly in small catchments and urban settings. Rainfall quantile estimates are used to understand and express the relationships between rainfall intensity, rainfall duration (aggregation scale), and the frequency of occurrence (probability of exceedance) of such rainfall events, also known as Rainfall Intensity-Duration-Frequency (IDF) curves (Cheng and AghaKouchak, 2014; Koutsoyiannis et al., 1998; Koutsoyiannis and Iliopoulou, 2022). In practice, these design rainfall frequency estimates are required by public authorities and civil engineers designing hydraulic structures (National Weather Service, 2022; Onderka et al., 2022, 2023; Poschlod et al., 2021). There are many uses of IDF curves; for example, de Michele et al. (2002) developed IDF curves for design storms, Yu et al. (2004) developed regional IDF formulas for non-recording sites in Taiwan; Molnar and Burlando (2005) examined scaling exponent variability in a mountainous region; Nhat et al. (2007) developed regional relationships for ungauged locations in Japan. Statistics of rainfall extremes also play a central role in the reliable prevention of soil erosion and the estimation of soil losses (Hlavčová et al., 2015; Onderka and Pecho, 2021; Onderka et al., 2022). How climate change will affect the occurrence of rainfall extremes in the future (Berg et al., 2019; Ganguli and Coulibaly, 2017) is therefore of crucial interest, since the atmosphere's water holding capacity depends on the raising air temperature. According to the Clausius-Clapeyron relation, the amount of precipitable water increases with the rising air temperature by about 7% per 1 °C (Berg et al., 2019; Ganguli and Coulibaly, 2017; Onderka and Pecho, 2021; Onderka et al., 2022).

Rainfall projections from Regional Climate Models (RCMs) provide information on how rainfall extremes may evolve in the future (Zhao et al., 2021). Rainfall extremes are regularly assessed using regional climate model simulations in daily time steps. However, shorter sub- daily extremes have received less research attention. This may be due to the lack of high-temporal resolution observations and model output data (Berg et al., 2019). Berg et al. (2019) processed EURO CORDEX 0.11° regional climate models to derive an ensemble of depth-duration-frequencies for Europe (1–12 hour durations). They found that at short durations, the depth-duration-frequencies are significantly underestimated. They observed temperature-precipitation scaling variations across Europe at ~1−10 % K−1 for 12-hour durations, and higher values for shorter durations. A recent study from the Netherlands revealed that sub-hourly precipitation extremes increased even above the Clausius–Clapeyron relation, which is a phenomenon described as super-CC scaling (Lenderink et al., 2017). Similar findings have also been reported from other regions of the world (Ban et al., 2015; Berg et al., 2019; Blenkinsop et al., 2015; Miao et al., 2015; Schroeer and Kirchengast, 2018; Shaw et al., 2011; Wasko and Sharma 2015, 2017). However, the rate at which rainfall extremes increase with rising air temperatures varies across different latitudes, and strong contrasts between regions are to be expected (Földes et al., 2022; Hlavčová et al., 2015; Onderka et

al., 2022; Szolgay et al., 2023; Vyshnevskyi and Shevchuk, 2022; Zhao et al., 2021). RCM climate simulations usually show systematic biases that have to be reduced before further applications. Bias correction approaches counteract the tendency of RCM simulations to overestimate or underestimate downscaled variables. RCM outputs must be bias corrected (BC) to be applicable to impact assessment studies. Many BC approaches adjust climate factors separately (univariate BC) or jointly (multivariate BC), see Ansari et al. (2023). Many bias correction methods have been proposed and applied in rainfall (and other meteorological variables) studies (Piani et al., 2010; Teutschbein and Seibert, 2013). Their main objective is to adjust the statistical characteristics of rainfall simulations to resemble those of historical baseline observations.

Using models from CORDEX-EA-II, Chen et al. (2022) examined linear scaling, distributional-based quantile mapping (QM), and empirical-based QM for surface air temperature and precipitation BC. They advised using BC approaches to carefully consider regional climate and research goals. Das and Zhang (2022) found that empirical quantile mapping for precipitation and maximum temperature BC and distribution mapping for minimum temperature BC performed better with CORDEX RCMs in Ethiopia. Derdour et al. (2022) examined four CORDEX RCMs for northeastern Algeria's precipitation. Gamma quantile mapping BC enhanced raw RCM averaged precipitation data in most time steps (annual, seasonal, monthly, and daily) significantly. As shown in the literature review below, numerous comparisons reveal that the application, projected data type, and regional climate should be considered when picking a method.

Dobor and Hlásny (2019) examined CORDEX bias-corrected climate simulations using MESAN re-analysis data from 1989–2010. They suggest using the bias correction period as a reference period. Gampe et al. (2019) employed the usual QM BC method to correct bias in 15 EURO-CORDEX regional climate model (RCM) simulations over northern Italy's Alpine Adige watershed. The BC reference dataset greatly affected future precipitation estimates. Ghimire et al. (2019) compared eight rainfall BC methods in Myanmar. Methods with monthly correction factors improved performance statistics.

According to Holthuijzen et al. (2022) empirical quantile mapping (QEM) can rectify distributional inconsistencies between simulated climatic variables and observed data, but it is sensitive to calibration periods and prone to overfitting. Ivanov and Kotlarski (2017) found that QM outperforms the delta change method in distribution-tail characteristics and temporal statistics and recommend QM for RCMs to local weather stations over an alpine terrain.

Lehner et al. (2020, 2023) have drawn attention to the fact that most existing bias correction techniques only focus on the bias in the mean value or on the extreme values separately. They recommend that the quantile that captures the bias best (whether in the mean or any extreme value) be determined for a specific location and investigated if it varies spatially and seasonally.

Ngai et al. (2022) considered seven bias-corrected regional climate models using QM from CORDEX-SEA over Southeast Asia with eleven rainfall indices and found that the QM procedure reduced biases and inter-model variations in a historical period. In a study of five regional climate models from the ENSEMBLES project in Europe from 1961–1990, Szabó-Takács et al. (2019) found that bias correction may vary according to the region of the model's domain.

Tootoonchi et al. (2023) contrasted advanced multivariate BC methods with two simple univariate methods for reproducing 16 hydrological signatures. The results showed that all the bias-adjustment strategies significantly decreased the biases and improved the consistency of the simulated hydrological signatures. The added value of the multivariate methods in maintaining the dependence structures between the precipitation and temperature was not systematically reflected in the resulting hydrological signatures, as they were generally outperformed by univariate methods.

As shown above, QM BC is popular when correcting systematic biases simulated by RCMs (Cannon et al., 2015; Osuch et al., 2016). Corrections can be done to the modeled mean, variance, higher moments, and quantiles of a distribution (Cannon et al., 2015). In the method, the transfer function between the rainfall simulations and observations is based on the cumulative distribution functions estimated from the observed and modelled values. Unfortunately, when a cumulative distribution function is applied to the entire series, the resulting bias-corrected data are skewed by the dominance of the non-extreme data. In order to maintain physical scaling of precipitation extremes with the temperature via the Clausius-Clapeyron equation, the bias correction should be able to preserve trends in the projected precipitation extremes. Usually, the parameters of the distributions in the quantile mapping method are assumed to be constant; however, due to changing climatic conditions, the assumption of stationarity may not be valid for extreme rainfall events, which is seldom explicitly considered (Cannon et al., 2015; Hempel et al., 2013; Hlavčová et al., 2015). Schmith et al. (2021) found that adjusting the hourly data from historical and RCP8.5 scenario runs from 19 EURO-CORDEX ensemble model simulations improves estimates of future return levels. On hourly timescales, the climatic factor technique outperformed QM. They also noted that the bias of the adjusted projected results may not match the future reality better, since the bias may not be stationary in a changing climate. Lehner et al. (2020) compared quantile mapping, scaled distribution mapping (SDM), and quantile delta mapping using Austrian daily temperature and precipitation data. QDM met the criterion to preserve long-term climatological trends of means (climate change signal).

According to Hui et al. (2020), BC approaches assume the bias stationarity of climate model results. Due to climate variability or change, this assumption may be incorrect. They suggested calibrating a bias correction strategy for hydrological climate change impact assessments over a long-term period to eliminate natural climate variability.

In studies on extreme hydrological and meteorological events, the Generalized Extreme Value (GEV) distribution is generally considered useful (Katz et al., 2002), since it is the limit distribution of the standardized maxima of the series of independent and identically distributed random variables. Quantile mapping was performed using many probability distribution models in South Korea by Shin et al. (2019). The results show that the gamma-Gumbel mixture distribution best reproduces the statistical characteristics of especially extreme precipitation by fitting the majority of non-severe precipitation events to the light-tailed gamma distribution and the extreme events to the Gumbel distribution.

Respecting trends in the data with GEV distribution is possible. For example, Ganguli and Coulibaly (2019) in the assessment of changes in intensity-duration-frequency curves in Canada considered parameters of the GEV as linear functions of time (Feitoza Silva et al., 2021).

In the recent past, alternative IDF relationship construction methods based on rainfall fractal features, which imply scaling invariances, were devised. Koutsoyiannis and Foufoula-Georgiou (1993) predicted storm hyetographs using a scaling

model, while Gupta and Waymire (1990) examined simple and multiple scaling to characterize the probabilistic structure of precipitation. Based on rainfall scaling features, scaling formulas were provided to extend IDF relationships from a typically daily time scale to shorter time intervals. Bendjoudi et al. (1997) employed a multifractal perspective on rainfall IDF curves, Rosso and Burlando (1990), and Burlando and Rosso (1996) studied classical depth-duration-frequency relationships. Menabde et al. (1999) showed that basic IDF relationships may be derived from empirically observed scaling features of rainfall and certain general assumptions regarding the cumulative distribution function for the annual maxima of mean rainfall intensity. De Michele et al. (2002) developed Intensity-Duration-Frequency (IDF) curves for design storms, while Yu et al. (2004) established regional IDF formulas for non-recording sites in Taiwan. Molnar and Burlando (2005) investigated the variability of scaling exponents in a mountainous region, and Nhat et al. (2007) derived regional relationships for ungauged locations in Japan.

These method continues to be used all over the world. Casas-Castillo et al. (2018, 2022) considered scaling properties of extreme rainfall in Madrid and Andalusia (Spain), while Diedhiou et al. (2024) applied simple scaling to an extreme precipitation regime in Senegal. In Slovakia, the scaling properties of extreme rainfall were first tested in Bara et al. (2008) and recently applied by Földes et al. (2022) in studying the impact of changes in short-term rainfall on design floods.

Intensive rainfall over Slovakia is mostly generated during westerly and north-westerly cyclonic situations arriving from the Atlantic Ocean and occasionally also from cyclonic situations from the Mediterranean or the Black Sea (Mészáros et al., 2022) or by convective events. Orography also affects daily rainfall totals (Bohuš et al., 1974; Mészáros et al., 2022; Šamaj, 1959). As for short-term rainfall, the effects of orography are not yet sufficiently understood (Mazzoglio et al., 2022). Onderka et al. (2023) applied a regularized spline with tension to grid local estimates of rainfall quantiles for durations of 5 minutes up to 24 hours using the elevation, longitude, and latitude as covariates. For 24-hour rainfall, the positive correlation with elevation was apparent, while for shorter durations, the elevation did not seem to play a significant role. Based on previous investigations of pluviographic observations in the Tatra Mountains, the highest hourly intensities occur in the northwest, where average hourly intensities range from 1 to 2 mm/h. On the southern slopes of the High Tatras, mean hourly rainfall intensities are much lower, ranging from 0.8 to 1.4 mm/h (Bohuš et al., 1974; Mészáros et al., 2022; Šamaj, 1959).

The particular objectives of this paper are: (1) to describe a novel bias-correction method applicable to non-stationary extreme series capable of preserving trends in climate model simulations; (2) to empirically downscale 3-hour quantiles derived from RCMs to temporal scales of 5 to 180 minutes using spatially differentiated downscaling functions (local empirical scaling functions); (3) to estimate quantiles of 5 to 180-minute rainfall calculated from EURO-CORDEX regional climate models for the time horizon of 2080 and calculate the relative changes in quantiles between the historical period of 1991–2021 in Slovakia.

2 MATERIAL AND METHODS

2.1 Regional climate models (RCMs)

To better understand the impact of climate change within any region investigated, it is crucial to consider several climate models that are representative of the area. Meitner et al. (2023) carried out a careful validation and selection of regional climate models that are most suitable for the region of Central Europe based on spatial and seasonal patterns. Following the findings and recommendations of Meitner et al. (2023), we selected several EURO-CORDEX RCMs as suitable candidates for further analyses (Table 1).

Table 1. List of regional climate models (RCMs) used to create multi-scenario EURO-CORDEX ensembles [GCM: MOHC-HadGEM2-ES (UK)].

RCM	Simulation
CNRM-ALADIN63 (France)	Historical [1991–2005]
SMHI-RCA4 (Sweden)	Historical [1991–2005]
DMI-HIRHAM5 (Denmark)	Historical [1991–2005]
KNMI-RACMO22E (the Netherlands)	Historical [1991–2005]
CNRM-ALADIN63 (France)	RCP8.5 [2006–2095]
SMHI-RCA4 (Sweden)	RCP8.5 [2006–2095]
DMI-HIRHAM5 (Denmark)	RCP8.5 [2006–2095]
KNMI-RACMO22E (the Netherlands)	RCP8.5 [2006–2095]

We used four RCMs with 3-hour precipitation simulations. The RCMs were downloaded from the Copernicus Data Store API (cds.climate.copernicus.eu). The RCM simulations of the accumulated precipitation are bound by "clock hours" at regular intervals (3-hour intervals).

The fundamental motivation of this paper is to detect changes in future extreme rainfall intensities. We have focused on the RCP8.5 scenario, since our objective was to estimate the rainfall quantiles corresponding to the most pessimistic emission scenarios. The input data cover the 1991–2021 historical period with rain gauge observations and the RCM simulations covering the 1991–2095 period.

2.2 Rain gauge data

Our analyses are restricted to the warm part of the year (April through October) to account for two facts. Firstly, most short-term rainfall extremes in the area investigated mostly occur during the warm part of the year; and secondly, mechanical self-registering rain gauges are designed to measure rainfall under non-freezing conditions (Onderka and Pecho, 2021; Onderka et al., 2022, 2023).

All the rainfall data observed at the rain gauges were obtained from the databases of the national weather service (Slovak Hydrometeorological Institute, Bratislava, Slovakia). The rain gauges are located throughout the entire study area at a broad range of altitudes, and their exact locations are shown in Fig. 1. Although there are data available from a total of 150 suitable rain gauges, only 75 locations fulfilled the criterion of a maximum 5 km distance between the rain gauge and the closest grid point centroid. The decision to limit the geographical distance to a maximum of 5 km was a compromise between an adequate number of pairs (RCM grid point | rain gauge) and the need to avoid coupling RCM grid points with rain gauges on the opposite side of a mountain barrier. Historical rain gauge observations from the period 1991–2021 were used for the bias correction and statistical downscaling of the 3-hour precipitation products of the EURO-CORDEX RCMs. Rainfall measurements were taken by two types of rain gauges: automatic instruments with a capture area of 200 cm^2 (TRws 214 manufactured by MPS System, Ltd.) and mechanical self-registering rain gauges with a capture area of 250 cm^2 (METRA manufactured in the former Czechoslovakia). The temporal resolution of the time series is 1 minute, while the resolution of the rainfall amounts is 0.1 mm. The processed data cover the period from 1991–2021.

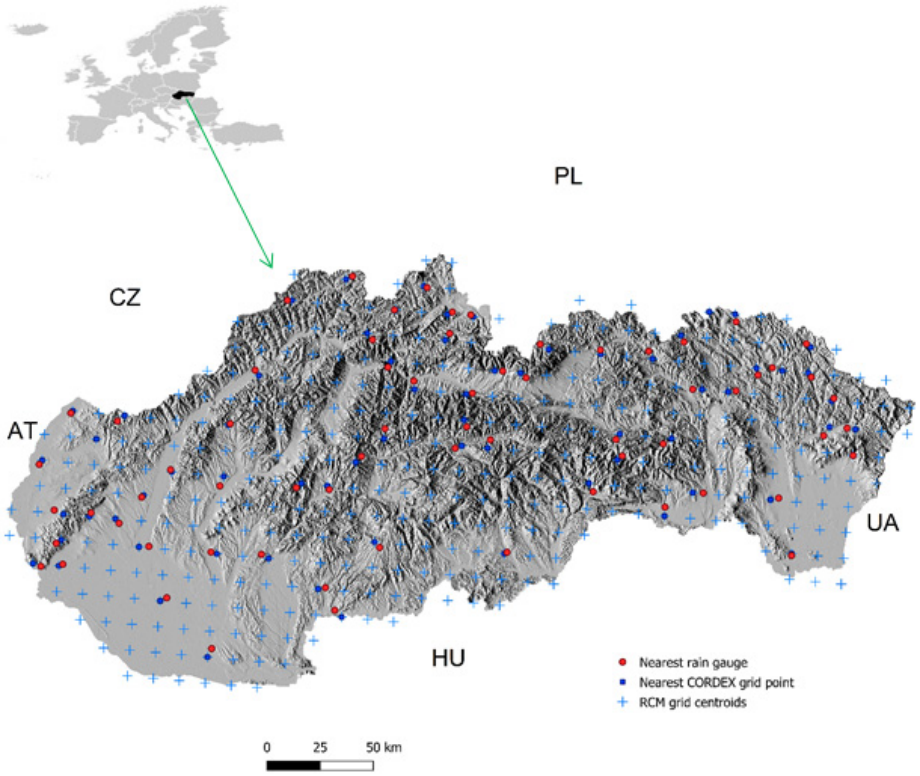

Fig. 1. Geographical locations of the rain gauges and the EURO-CORDEX grid points within the area investigated (Slovakia, Europe) that fulfil the criterion of a maximum 5 km distance.

2.3 Methodology

The methodology is divided into individual stages of data processing for both the rain gauge data and RCM data (Fig. 2), and this dataset was used for the subsequent analyses and bias corrections.

2.3.1 Data selection: annual maximum series

The raw quality-checked rainfall data with a 1-minute temporal resolution were aggregated (application of moving sums) to 5, 10, 15, 30, 40, 50, 60, 120 and 180 minutes. The annual maximum series was computed for each location and all the aggregation scales. The annual maxima series (75 locations × 9 aggregation scales) were used to fit the GEV distributions. Similarly, a series of annual maxima were constructed for each grid point separately for each RCM simulation of 3-hour accumulation precipitation rates.

2.3.2 GEV distribution: stationary case

The frequency of the occurrence of a rare meteorological or hydrological event is defined in terms of the annual exceedance probability or average return period, i.e., here, a probability associated with exceeding a given rainfall intensity for a specified duration at least once a year (Coles, 2001; Singh, 2016). In the case of stationary data, the cumulative distribution function $F(x)$ for the GEV distribution is defined as:

$$F(x) = \exp\left[-\left(1+\xi\left(\frac{x-\mu}{\sigma}\right)\right)^{\frac{-1}{\xi}}\right] \quad (1)$$

where μ is the location parameter; σ is the scale parameter; and ξ is the shape parameter describing the tail behavior of the GEV distribution (Cheng and AghaKouchak, 2014; Coles, 2001; Koutsoyiannis and Iliopoulou, 2022; Ragno et al., 2019). When ξ approaches zero, the GEV distribution becomes a Gumbel distribution; for $\xi < 0$, it corresponds to a reversed Weibull distribution, and for $\xi > 0$, to the Fréchet distribution (Coles, 2001). There are several methods as to how to estimate the parameters of the GEV distribution. Among the most common techniques are the maximum likelihood estimation, the least squares method, the method of moments, and the Bayesian inference (Coles, 2001; Onderka et al., 2022, 2023). The Bayesian inference of distribution parameters is robust against issues of short-term series (Coles, 2001). If we know the parameters of F, then the estimated values of the extreme quantiles of the annual maxima can be determined from the inverse function of F, namely:

$$x = \mu - \frac{\sigma}{\xi}[1-\{-\ln(1-p)\}^{-\xi}] \quad (2)$$

where x is the quantile of rainfall intensity corresponding to the probability of exceedance equal to p. The quantile x can therefore be thought of as a rainfall intensity (annual maxima), which is expected to be reached or exceeded in every single year with the probability p. The quantile x can therefore be thought of as a rainfall intensity that is expected to be exceeded, on average, every T years, where $T = \frac{1}{p}$. The parameters of the GEV distribution were estimated by the Bayesian approach with a Markov Chain Monte Carlo (MCMC) sampling (AghaKouchak et al., 2013; Onderka et al., 2022, 2023; Ragno et al., 2019). More details on the inferences of GEV parameters can be found in the recently published papers of Onderka et al. (2022, 2023).

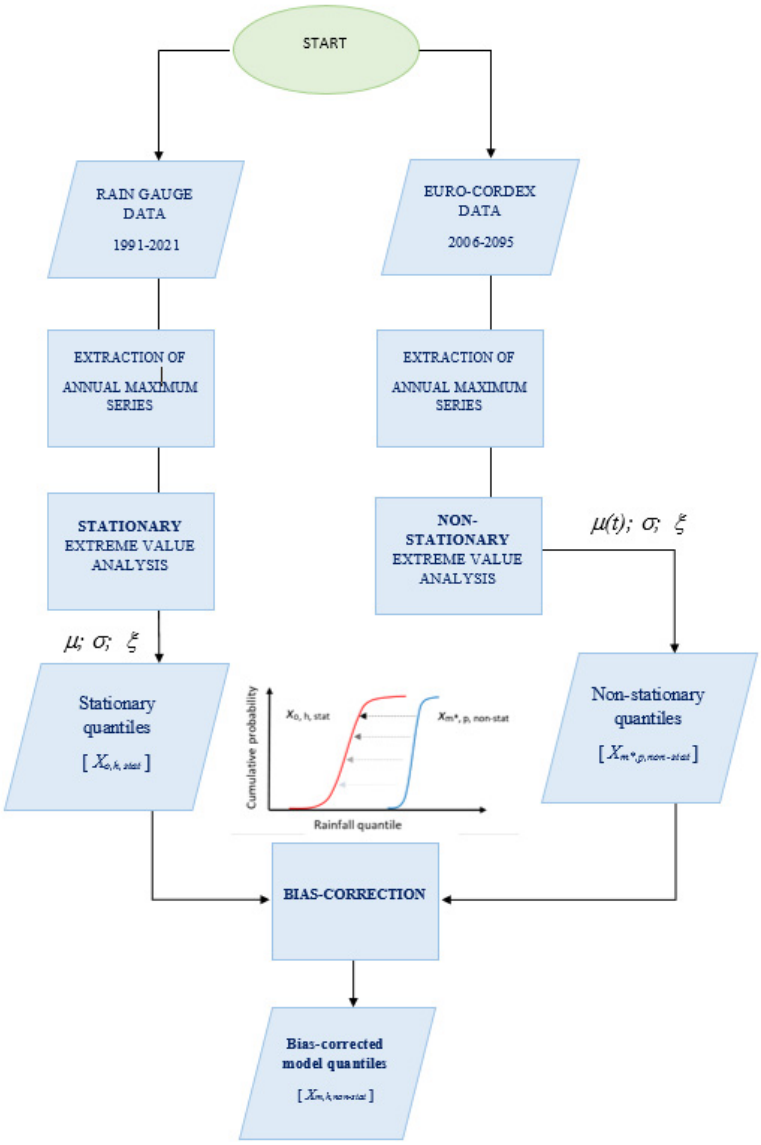

Fig. 2. Flow chart representing the individual data processing stages for both the rain gauge data and RCM data.

2.3.3 GEV distribution: non-stationary case

Using daily EURO-CORDEX RCMs, Hosseinzadehtalaei et al. (2018) found that the assumption of temporal stationarity in a rainfall series leads to the severe underestimation of rainfall intensity quantiles. The bias correction technique presented is based on the concept of time-varying quantiles proposed by Katz et al. (2002). A time-varying quantile x varies over time or any other physically meaningful covariate (e.g., air temperature, humidity, CO_2 concentrations, etc.). However, the time-varying quantile can be interpreted in a similar way as '*stationary*' quantiles derived under a stationarity assumption (AghaKouchak et al., 2013; Katz et al., 2002).

In this paper, the stationary GEV (Eq. 1) is extended to account for non-stationarity by introducing additional functional relationships between the distribution parameters and time as a covariate. The non-stationary formulation of Eq. (1) can thus be written for a linear function of time (as a special case of a linear temporal trend) as:

$$F_{NS}(x) = \exp\left[-\left(1+\xi(t)\left(\frac{x-\mu(t)}{\sigma(t)}\right)\right)^{-\frac{1}{\xi(t)}}\right] \quad (3)$$

where $\mu(t)$ is the time-dependent location parameter $\mu(t) = \mu_0 + \mu_1 t$, $\sigma(t)$; is the time-dependent scale parameter $\sigma(t) = \sigma_0 + \sigma_1 t$; and ξ is the time-dependent shape parameter $\xi(t) = \xi_0 + \xi_1 t$. The parameter μ_1 can be visualized as the slope of a linear trend in the center of the distribution (see the upper panel in Fig. 3). First, the observed data were used to find the annual maximum series for each rain gauge. Likewise, the annual maximum series were found for each of the model grid points within the modeled region (Fig. 1). The historical rainfall quantiles were calculated for each rain gauge using the estimated parameters of the GEV distribution (stationary case, Eq. 2). Next, the quantiles of the same orders were estimated for each of the model grid points by applying the non-stationary form of the GEV distribution for a 3-hour interval (Eq. 3).

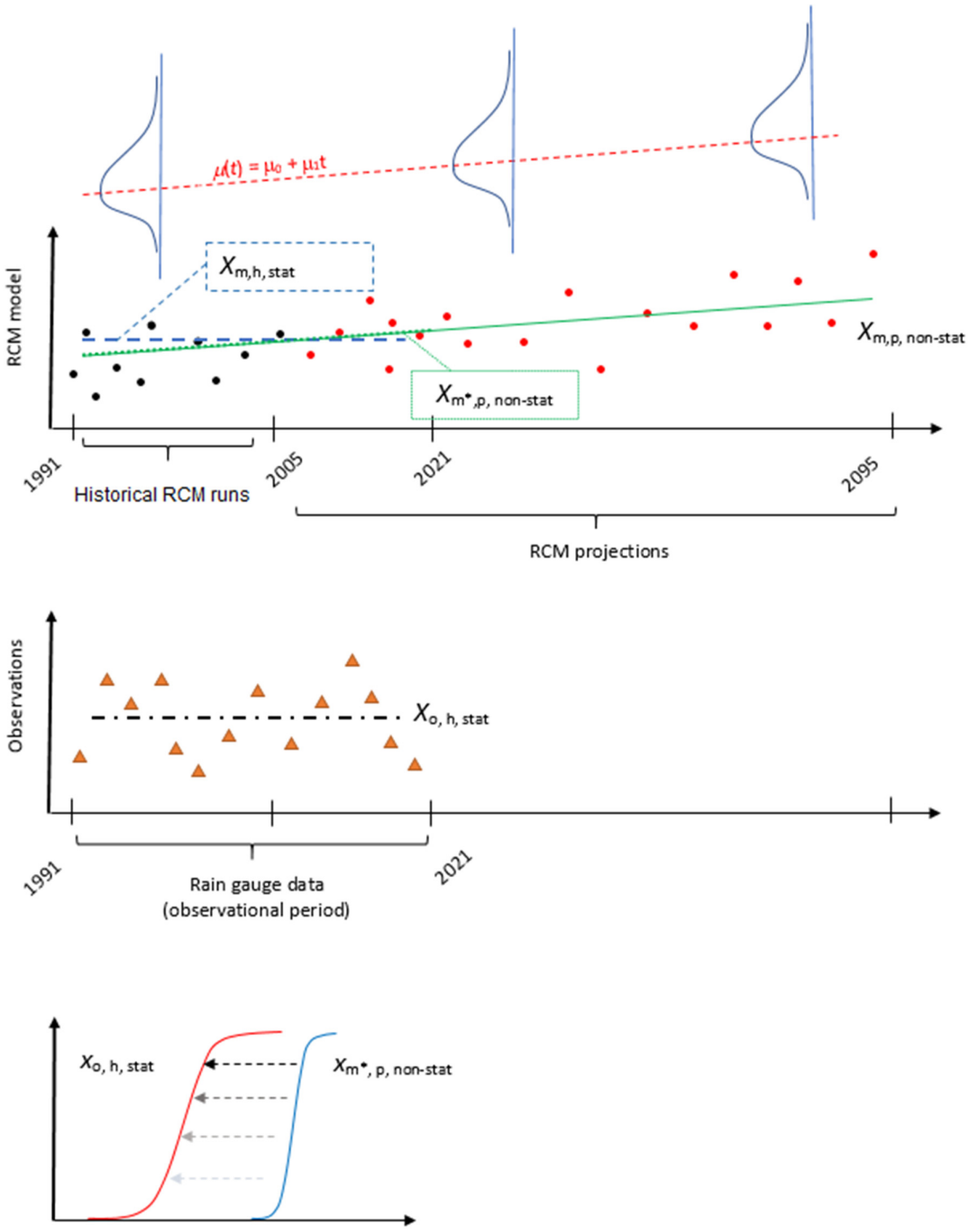

Fig. 3. Conceptual representation of a non-stationary series featuring the time-dependent location parameter of the GEV distribution, denoted as $\mu(t) = \mu_0 + \mu_1 t$. The upper section displays a non-stationary hypothetical quantile derived from RCM simulations, combining both the historical RCM runs ($x_{m*,p,non-stat}$) and the RCM projections ($x_{m,p,non-stat}$), where the term $x_{m,h,stat}$ equals the $x_{m*,p,non-stat}$ exactly at the center of the historical time series. The middle section illustrates a stationary model portraying a hypothetical quantile based on the data observed during the period 1991–2021 ($x_{o,h,stat}$). The lower section illustrates the principle of the simple quantile mapping of $x_{m*,p,non-stat}$ into $x_{o,h,stat}$.

2.3.4 Bias-correction under non-stationary climate conditions

To prove the need for bias correction in rainfall quantiles, we compared the RCM-based quantiles (prior to the bias correction) with the quantiles derived from historical observations for the period 1991–2021. The relative differences between the rainfall quantiles derived from the four RCMs and rain gauge data prior to the bias correction were expressed for each specific return period as:

$$\Delta\% = 100\left(\frac{x_r}{x_m} - 1\right) \quad (4)$$

where x_r is the quantile estimated from the rain gauge data (d = 180 min), and x_m is the quantile of the same order estimated from the RCM simulations of a 3-hour rainfall. The relative differences show how much the estimated RCM quantiles deviate from the quantiles observed in the rain gauge data without any bias correction.

Most bias correction approaches replicate the probability distribution of a model to observations using variations of the quantile mapping approach (Haerter et al., 2011; Johnson and Sharma, 2012; Lin et al., 2019; Mehrotra and Sharma, 2012, 2019; Nguyen et al., 2016; Teutschbein and Seibert, 2013; Wood et al., 2004; Zhao et al., 2021). Quantile mapping can be mathematically described as a transfer function:

$$q_{m,p}(t) = F_{o,h}^{-1}\{F_{m,t_1}[x_{m,p}(t)]\} \quad (5)$$

where $q_{m,p}(t)$ is the bias-corrected quantile of the annual maximum series modelled for a time t within some projected period (denoted by the subscripts m and p); $F_{o,h}^{-1}$ is the inverse cumulative distribution function (CDF) of the historical observations; F_{m,t_1} is the CDF of the modelled projected data for time t_1; and $x_{m,p}(t)$ is a modeled value at time t within some projected period.

The assumption in fitting a distribution function to rainfall intensities is that the time series is strictly stationary. However, this assumption is not satisfied in changing climate conditions. Under non-stationary conditions, the quantile mapping approach described in the previous paragraph may not be adequate for preserving trends. Since traditional bias-correction techniques (e.g., quantile mapping, delta quantile mapping, etc.) are fundamentally designed to correct the entire distribution function, the resulting bias-corrected data are inevitably skewed by the dominance of the non-extreme data. To avoid this problem, we propose a novel technique based on a non-stationary form of the GEV distribution that allows us to map quantiles from the upper tail of the GEV distribution where all the extremes are located (Holthuijzen et al., 2022; Ivanov and Kotlarski, 2017; Lehner et al., 2020, 2023).

The proposed approach for non-stationary bias correction is outlined below. The mathematical framework is based on the non-stationary formulation of the GEV distribution (Eq. 3). The location parameter μ was allowed to vary over time as $\mu(t) = \mu_0 + \mu_1 t$. Given the relatively limited length of the annual maximum series of observed rainfall (30 years), we assume that the scale parameter σ and the shape parameter ξ of the GEV distributions are stationary. Allowing the location parameter μ to vary over time as $\mu(t) = \mu_0 + \mu_1 t$, and assuming the parameters σ and ξ are kept constant, the quantile of the nonstationary GEV distribution ($x_{m*,p,non\text{-}stat}$) matches the quantile of the stationary GEV distribution ($x_{m,h,stat}$) precisely at the series' central point. This property is depicted in the upper section of Fig. 2 (upper section), where the non-stationary quantile intersects the stationary quantile at the midpoint of the 1991–2021 period. In other words, the value of the non-stationary quantile at the midpoint of the 1991–2021 period corresponds to the stationary quantile derived for the entire 1991–2021 period. However, it is important to note that this equivalence would not hold if the σ and ξ parameters were permitted to vary over time or if the location parameter $\mu(t)$ was handled as a nonlinear function.

The stationary quantiles ($x_{m,h,stat}$) were computed using the historical rain gauge observations according to Eq. (2). Having the estimated stationary quantiles from the historical 1991–2021 period, we can move forward with the quantile mapping (Fig. 3).

$$q_{m*,p,non-stat} = F_{o,h,stat}^{-1}\{F_{m*,p,non-stat}[x_{m,p,non-stat}]\} \quad (6)$$

where $q_{m*,p,non-stat}$ is the bias-corrected quantile of the value modeled at the center of the observational period (i.e., 2006, for the observational period starting in 1991 and ending in 2021); $F_{o,h,stat}^{-1}$ is the inverse CDF of the historical 'stationary' observations; $F_{m*,p,non-stat}$ is the CDF of the modeled value at time t_1; and $x_{m,p,nan-stat}$ is the predicted value modeled at a future time t.

2.3.5 Empirical downscaling of 3-hour RCM rainfall quantiles

The 3-hour quantiles of rainfall (bias-corrected RCM quantiles) were empirically downscaled to shorter aggregation levels (durations d) using empirical scaling parameters. The empirical scaling parameters were derived for each rain gauge and return periods T_r = 2, 5, 10, 20, 30, 50 and 100 years. The empirical scaling parameters were calculated as the ratio of the 180-minute quantile and quantiles corresponding to durations d from 5 to 120 minutes:

$$k_d = \frac{q_{180}}{q_i} \quad (7)$$

where q_{180} (mm min^{-1}) is the quantile for 180-minute rainfall intensities derived from the closest rain gauge (within a maximum distance of 5 km); q_i (mm min^{-1}) is the quantile for a rainfall intensity of duration d. It should be noted here that the scaling parameters were computed based on the historical (observed) period.

Assuming that the scaling parameters will be valid in a future climate, the 3-hour rainfall quantiles calculated from the RCMs can be downscaled to lower aggregation scales (5- to 180- minute rainfall durations (d)) by applying Eq. (7). In the final step, the bias-corrected quantiles previously estimated from the four RCMs and downscaled to quantiles for 5- to 180-minute durations were further processed to obtain the median values (an ensemble).

3 RESULTS

We have analyzed four regional climate models and corrected their systematic biases using rain gauge data for the historical period 1991–2021. The relative differences between the rainfall quantiles derived from the four RCMs and the rain gauge data prior to the bias correction expressed for each specific return period (Eq. 4) are shown in Fig. 4 for a single location (an example generated for the grid point closest to the Bratislava airport).

Fig. 5 shows the differences as boxplots for each RCM separately. In general, quantiles estimated from RCMs tend to be higher than the quantiles derived from the rain gauge series. It follows from Eq. (4) that a percentage above zero indicates that the quantile estimated for the rain gauge data is higher than the quantile estimated for the closest RCM grid point. The uncorrected RCM-based quantiles are underestimated by the RACMO22E, ALADIN63, and RCA4 models, while the HIRHAM5 model tends to overestimate the quantiles.

The non-stationary form of the GEV distribution was used to estimate the rainfall quantiles for both the historical and future horizons, the rain gauge data, and the RCM simulations. The rainfall quantiles for durations of 5 to 180-minutes were estimated using locally-derived empirical scaling parameters.

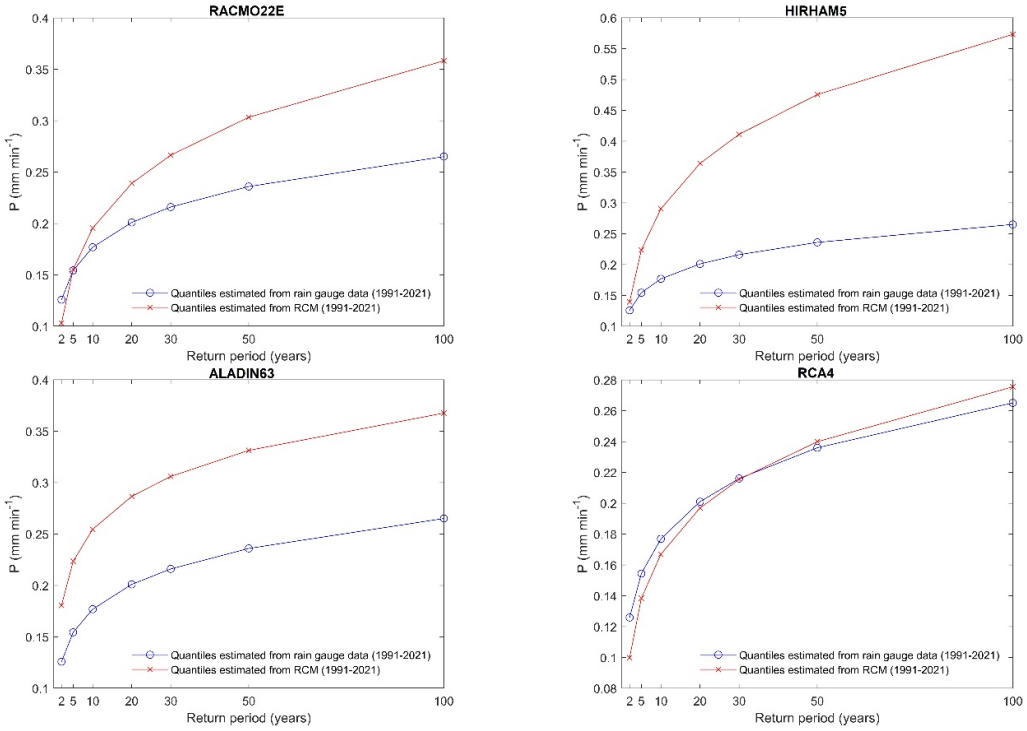

Fig. 4. Uncorrected rainfall quantiles (d = 3 hours) derived from four RCMs (ALADIN63, HIRMAHM5, RACMO22E and RCA4) and quantiles derived from rain gauge data (d = 180 min). The example was generated from the grid point closest to the rain gauge at the Bratislava airport.

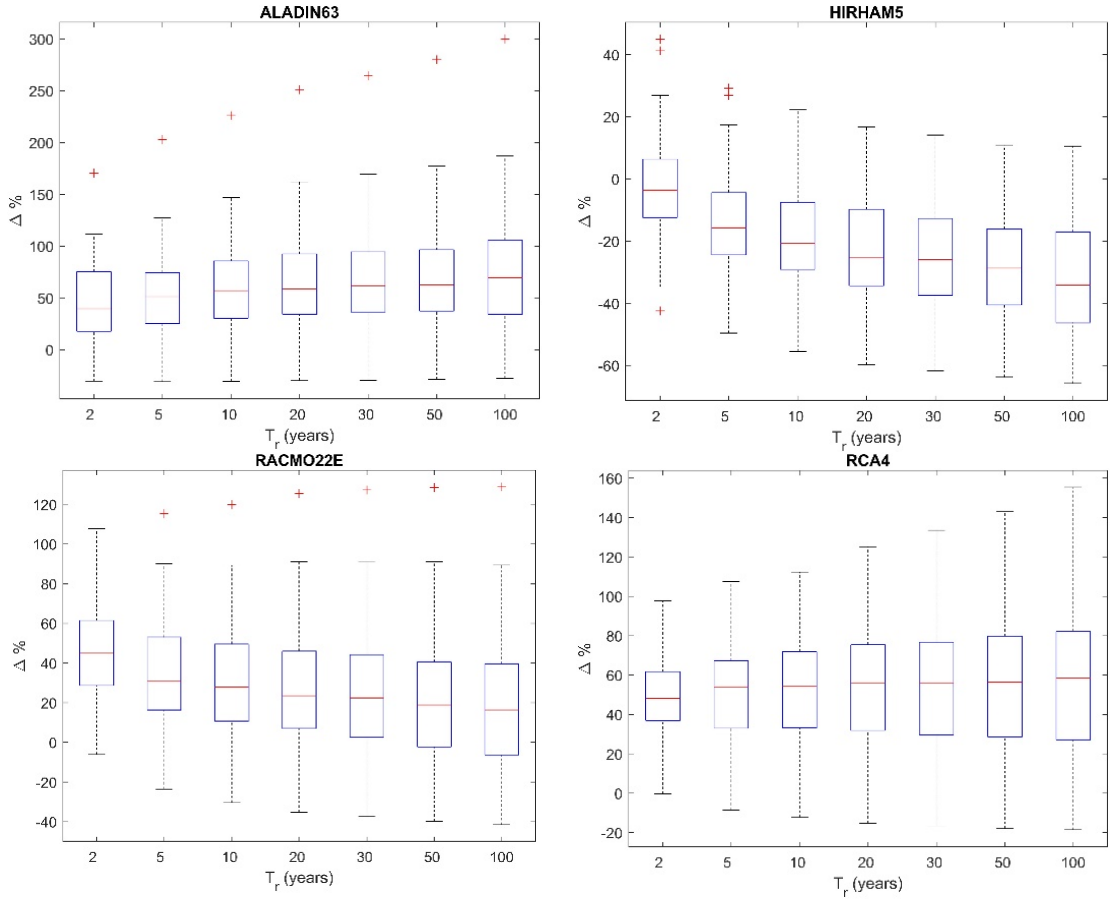

Fig. 5. Boxplots illustrating the spread of the relative differences (prior to the bias correction) between the 3-hour RCM-based quantiles and the 180-minute quantiles derived from the 1991–2021 historical observations (N = 75). The straight red lines represent the median values.

The local scaling parameters k_d (Eq. 7) were derived for each rain gauge separately. A total of 75 scaling functions were established. A summary of the statistics of the scaling parameters are provided in Table 2 and visualized in Fig. 6.

The empirical scaling parameters were calculated using (Eq. 7). The top and bottom edges of each box are the upper (75^{th}) and lower (25^{th}) quartiles, respectively. The distance between the top and bottom edges is the interquartile range (IQR). The outliers are indicated as + symbols. The whiskers are the lines that extend above and below each box.

Estimates of future rainfall quantiles based on the RCM simulations were subsequently downscaled using the empirical scaling function from the locations that met the criterion of a 5 km proximity. However, a disadvantage of using a local scaling function is the assumption made about its validity in future climates. In this paper, we present the results for the horizon of 2080 to show how future quantiles of rainfall are likely to evolve in the distant future. The relative change in rainfall quantiles between the historical period 1991–2021 and the time horizon of 2080 is associated with the return period, as summarized in Table 3.

For the return periods $T_r = 2$ years, the average of the relative changes that were calculated for the whole set of grid points is 13.5% (st. dev.: 2.9%). The relative change tends to decline with the increasing return periods. Concerning the longest return periods of 50 years and 100 years, the relative change is 5.5% (st. dev.: 1.1%) and 4.8% (st. dev.: 1%), respectively. The relative changes in the 2-year quantiles of rainfall for the grid points analyzed are shown in Fig. 7.

Particularly high relative changes in the 2-year rainfall quantiles are discernible in the mountainous areas, especially in the northern and north-eastern portions of the study region (Fig. 7). It is not the aim of this paper to clarify the spatial patterns in the short-term rainfall quantiles and their associated

Table 2. Summary of the statistics of the empirical downscaling parameters k_d for rainfall durations d ranging from 5 to 180 minutes ($N = 75$). P10 and P90 stand for the 10^{th} and 90^{th} percentiles, respectively.

	***d* (min)**										
	5	**10**	**15**	**20**	**30**	**40**	**50**	**60**	**90**	**120**	**180**
Min.	0.056	0.085	0.112	0.139	0.194	0.248	0.302	0.356	0.514	0.624	1
Max.	0.215	0.237	0.261	0.307	0.384	0.455	0.520	0.564	0.696	0.813	1
Median	0.095	0.129	0.160	0.190	0.248	0.302	0.357	0.410	0.565	0.714	1
Std.dev.	0.023	0.024	0.026	0.027	0.029	0.031	0.033	0.032	0.029	0.024	1
P10	0.072	0.104	0.135	0.163	0.219	0.274	0.325	0.378	0.534	0.689	1
P90	0.128	0.159	0.192	0.226	0.292	0.352	0.409	0.457	0.606	0.746	1

Table 3. Summary of the statistics of the relative changes (%) in quantiles between the historical period 1991–2021 and the horizon 2080.

	***T*r (years)**						
	2	**5**	**10**	**20**	**30**	**50**	**100**
Average	13.5%	9.7%	8.0%	6.7%	6.2%	5.5%	4.8%
Minimum	7.2%	5.4%	4.6%	3.9%	3.6%	3.2%	2.7%
Maximum	19.1%	13.5%	11.2%	9.6%	8.8%	7.9%	7.0%
St. dev.	2.9%	2.0%	1.6%	1.3%	1.2%	1.1%	1.0%

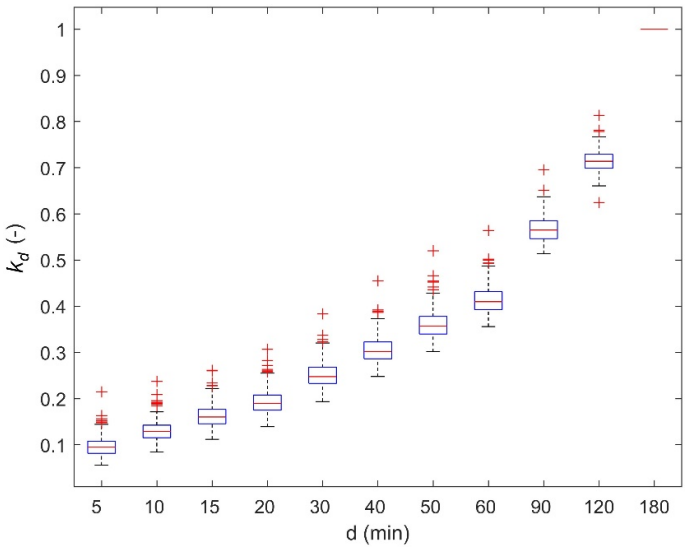

Fig. 6. Boxplots showing the empirical scaling parameters for rainfall intensities of 5- to 180-minute durations derived for all 75 locations that are equipped with rain gauges ($Tr = 2$ years).

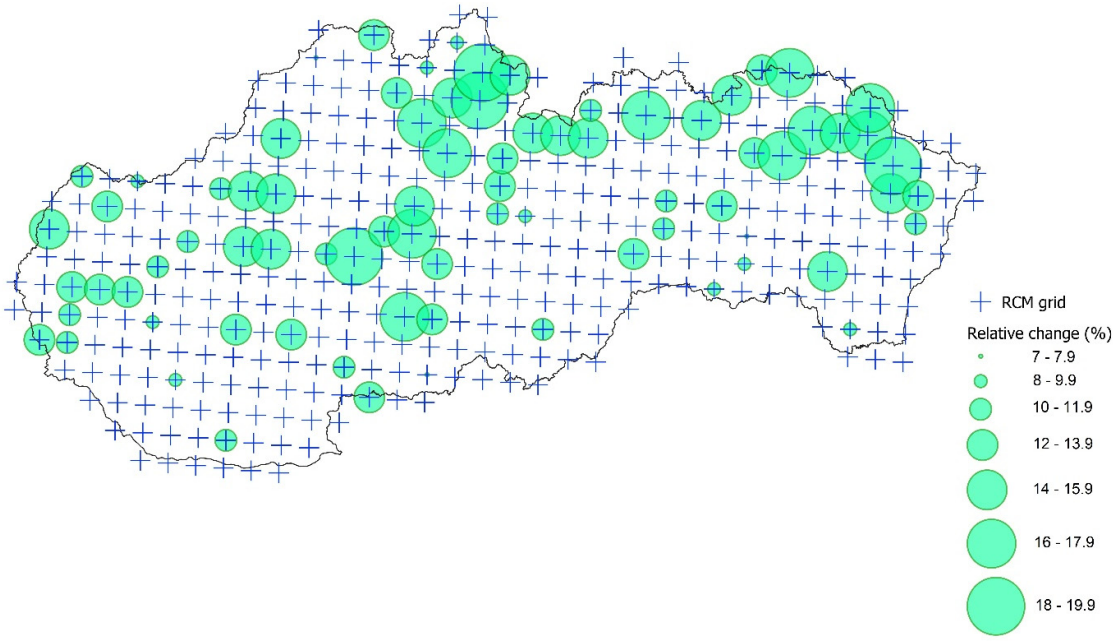

Fig. 7. Map of relative changes in the T_r = 2 years estimates of the rainfall quantiles between the historical period 1991–2021 and the time horizon 2080. Only grid points within a maximum distance of 5 km to the nearest rain gauge are shown on the map.

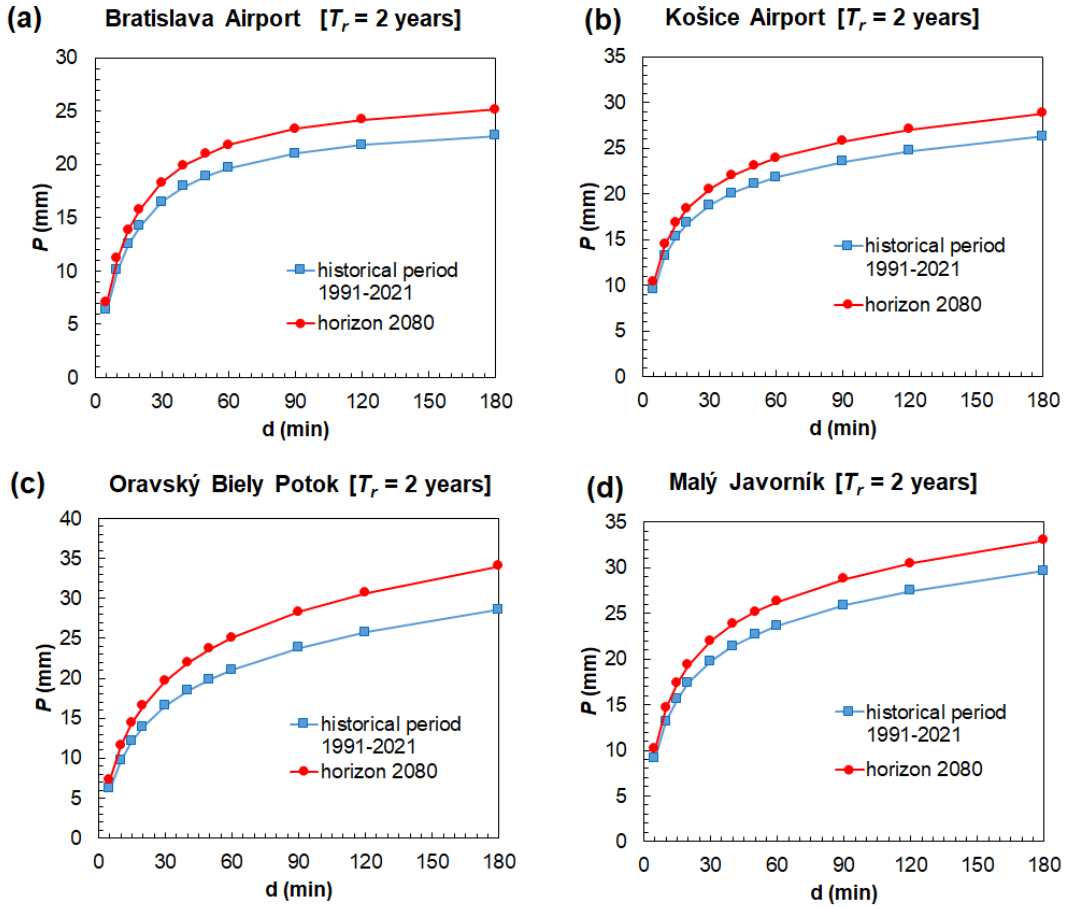

Fig. 8. Absolute changes in the rainfall quantiles (return period T_r = 2 years) between the historical period 1991–2021 and the future projection horizon of 2080 at the four rain gauges selected: (a) Bratislava airport; (b) Košice airport; (c) Oravský Biely Potok, and (d) Malý Javorník. The quantiles are shown as rainfall accumulations P (mm) over time scales (durations) d.

relative changes. Nevertheless, a detailed analysis of the spatial patterns in the rainfall quantiles remains an interesting avenue for further investigations in the future. This example shows an increase in the 2-year rainfall quantiles at the four locations. Finally, Fig. 8 illustrates how rainfall quantiles corresponding to the return period T_r = 2 years at the four sites selected differ between the historical observation period 1991–2021 and the projected future horizon 2080.

4 DISCUSSION

There is a consensus among climatologists that the recent increase in the global mean temperature is affected by cumulative emissions of greenhouse gases and the climate system feedback (Schwalm et al., 2020). According to recent measurements conducted by NOAA's Global Monitoring Laboratory (https://www.noaa.gov/news-release/greenhouse-gases-continued-to-increase-rapidly-in-2022), concentrations of greenhouse gases have increased on a global scale. For instance, carbon dioxide concentrations have increased to 417 ppm, which is a 50% increase compared to the pre-industrial levels. Future changes in the climate reflect both recent human activities and natural long-term climate variability. The Intergovernmental Panel on Climate Change (IPCC) Assessment Report described Representative Concentration Pathways (RCPs) as scenarios RCP2.6, RCP4.5, RCP6.0 and RCP8.5. The RCP scenarios use historical greenhouse gas emissions prior to 2005 and projected emissions subsequently (i.e., 2006 onwards). We have focused on the RCP8.5, oftentimes called the 'business as usual' scenario or the most pessimistic scenario. The RCP8.5 corresponds to an additional 8.5 W/m^2 radiative forcing by 2100, relative to pre-industrial conditions. According to a recent meta-analysis conducted by Friedlingstein et al. (2022), the RCP8.5 agrees within 1% with the total cumulative CO_2 emissions measured over the period 2005 to 2020. On the other hand, the RCP2.6 scenario underestimates the historically measured cumulative emissions by 7.4%. During the previous decade (2011–2020), the atmospheric CO^2 increased at a rate of ~5.1 GtC per year with a total of 47 % in CO^2 emissions (Friedlingstein et al., 2022). As discussed by Friedlingstein et al. (2022), the RCP8.5 can be considered as the most suitable scenario to describe the period 2005–2020. The RCP2.6 and RCP4.5 scenarios therefore retrospectively describe carbon dioxide emissions levels that did not occur.

A novel bias-correcting method based on the non-stationary form of the GEV distribution function has been described. Since sub-hourly rainfall intensities are perhaps the most important information for hydrological modeling in urban areas and small catchments, our attempt to estimate rainfall quantile intensities for time scales below 180 minutes is highly relevant. Local scaling relationships between 180-minute quantiles and quantiles corresponding to 5-, 10-, 20, 30-, 40-, 50-, 60-, 90-, and 120-minute rainfall were established for 75 locations equipped with rain gauges. The goal was to use the proposed non-stationary quantile mapping technique, as an example, to estimate return levels for rainfall intensities with durations ranging from 5 minutes to 180 minutes for the future horizon of 2080. Our results suggest that by the year 2080, rainfall intensities (2-year return period) may increase by ~10 to 20% compared to the 1991–2021 reference period (RCP 8.5 scenario). The relative change in rainfall quantiles between the historical period 1991–2021 and the time horizon of 2080 generally decreases with the return period. At the longest return period of 100 years, the relative change indicates an increase in rainfall quantiles by 4.8% (st. dev.: 1%). Whether this figure is large enough to pose significant consequences for the hydraulic infrastructure in urban areas is a question that remains to be answered. Nevertheless, this increase in rainfall quantiles is physically attributable to the Clausius-Clapeyron relationship, which is often interpreted as the CC-scaling of precipitation to the air temperature (Ban et al., 2015; Berg et al., 2019; Blenkinsop et al., 2015; Lenderink et al., 2017; Miao et al., 2015; Onderka and Pecho, 2021). Although Poschlod et al. (2021) presented 10-year rainfall return levels of hourly to 24-hour rainfall totals with a spatial resolution of 12.5 km for 16 European countries, Slovakia was unfortunately not included in their paper. Berg et al. (2019) processed four EURO-CORDEX 0.11° regional climate models to derive an ensemble of depth-duration-frequencies for Europe (1- to 12-hour durations). They found that at short durations the depth-duration-frequencies are significantly underestimated. They observed temperature-precipitation scaling variations across Europe at ~1−10 % K^{-1} for the 12-hour durations and higher values for shorter durations. The results presented here, therefore, are unique in that they fill in this gap and are, to our best knowledge, the first study conducted with regional climate models to estimate changes in sub-daily rainfall quantiles for Slovakia.

5 CONCLUSIONS

The main results of this paper can be summarized as follows:

- a procedure has been described that permits correcting extreme values (described by the upper tails of the GEV distribution), while preserving the trend in projected short-term rainfall extremes,
- the linear form of the non-stationary GEV distribution permits calculating quantiles for any future horizon,
- the bias correction technique presented preserves trends, i.e., it enables maintaining physical scaling with temperature projections through the CC-scaling relationship,
- the relative change in rainfall quantiles between the historical period 1991–2021 and the time horizon 2080 is 13.5% (st. dev.: 2.9%) for a return period of two years. The relative change tends to decline with increasing return periods. Concerning the longest return periods of 50 years and 100 years, the relative change is 5.5% (st. dev.: 1.1%) and 4.8% (st. dev.: 1%), respectively.

Acknowledgements. This work was supported by the Slovak Research and Development Agency (No. APVV 19-0340, No. APVV 20-0374, No. APVV 23-0332) and the VEGA Grant Agency (1/0782/21).

RERENCES

AghaKouchak, A., Easterling, D., Hsu, K., Schubert, S., Sorooshian, S. (Eds.), 2013. Extremes in a changing climate: detection, analysis and uncertainty. Water Science and Technology Library, 65. Springer Dordrecht, 426 p. ISBN 978-94-007-4478-3

Ansari, R., Casanueva, A., Liaqat, M.U., Grossi, G., 2023. Evaluation of bias correction methods for a multivariate drought index: case study of the Upper Jhelum Basin. Geosci. Model Dev., 16, 7, 2055–2076. https://doi.org/10.5194/gmd-16-2055-2023

Bara, M., Gaál, L., Kohnová, S., Szolgay, J., Hlavčová, K., 2008. Simple scaling of extreme rainfall in Slovakia: a case study. Meteorologický Časopis/Meteorol. J., 11, 4, 153–157.

Ban, N., Schmidli, J., Schär, C., 2015. Heavy rainfall in a changing climate: Does short-term summer rainfall increase

faster? Geophys. Res. Lett., 42, 4, 1165–1172. https://doi.org/10.1002/2014GL062588

Bendjoudi, H., Hubert, P., Schertzer, D., Lovejoy, S., 1997. Multifractal point of view on rainfall intensity–duration–frequency curves. C. R. Acad. Sci. Paris Earth Planet. Sci., 5, 325, 323–326 (in French)

Berg, P., Christensen, O.B., Klehmet, K., Lenderink, G., Olsson, J., Teichmann, C., Yang, W., 2019. Summer time precipitation extremes in a EURO-CORDEX 0.11° ensemble at an hourly resolution, Nat. Hazards Earth Syst. Sci., 19, 4, 957–971. https://doi.org/10.5194/nhess-19-957-2019

Blenkinsop, S., Chan, S.C., Kendon, E.J., Roberts, N.M., Fowler, H.J., 2015. Temperature influences on intense UK hourly precipitation and dependency on large-scale circulation. Environ. Res. Let., 10, 5, 054021. https://doi.org/10.1088/1748-9326/10/5/054021

Bohuš, I., Briedoň, V., Chomicz, K., Intribus, R., Kňazovický, L., Kolodziejek, M., Konček, M., Kurpelová, M., Murínová, G., Myczkowski, S., Orlicz, M., Orliczowa, J., Otruba, J., Pacl, J., Peterka, V., Petrovič, Š., Plesník, P., Pulina, M., Smolen, F., Sokolowska, J., Šamaj, F., Tomlain, J., Volfová, E., Wiszniewski, W., Wit-Jóźwikowa, K., Zych, S., Žák, B., 1974. The Climate of the Tatras. Veda, Bratislava, 856 p. (In Slovak.)

Burlando, P., Rosso, R., 1996. Scaling and multiscaling models of depth-duration-frequency curves for storm precipitation. J. Hydrol., 187, 1–2, 45–64. https://doi.org/10.1016/S0022-1694(96)03086-7

Cannon, A.J., Sobie, S.R., Murdock, T.Q., 2015. Bias correction of GCM precipitation by quantile mapping: how well do methods preserve changes in quantiles and extremes? J. Climate, 28, 17, 6938–6959. https://doi.org/10.1175/JCLI-D-14-00754.1

Casas-Castillo, M.d.C., Rodríguez-Solà, R., Llabrés-Brustenga, A., García-Marín, A.P., Estévez, J., Navarro, X., 2022. A simple scaling analysis of rainfall in Andalusia (Spain) under different precipitation regimes. Water, 14, 8, 1303. https://doi.org/10.3390/w14081303

Casas-Castillo, M.d.C., Rodríguez-Solà, R., Navarro, X., Russo, B., Lastra, A., González, P., Redaño, A., 2018. On the consideration of scaling properties of extreme rainfall in Madrid (Spain) for developing a generalized intensity-duration-frequency equation and assessing probable maximum precipitation estimates. Theor. Appl. Climatol., 131, 573–580. https://doi.org/10.1007/s00704-016-1998-0

Coles, S., 2001. An Introduction to Statistical Modeling of Extreme Values. Springer Series in Statistics. Springer-Verlag. https://doi.org/10.1007/978-1-4471-3675-0

Das, P., Zhang, Z., Ren, H., 2022. Evaluation of four bias correction methods and random forest model for climate change projection in the Mara River Basin, East Africa. J. Water Clim. Change, 13, 4, 1900–1919. https://doi.org/10.2166/wcc.2022.299

De Michele, C., Kottegoda, N.T., Rosso, R., 2002. IDAF (intensity-duration-area frequency) curves of extreme storm rainfall: a scaling approach. Water Sci. Technol., 45, 2, 83–90. https://doi.org/10.2166/wst.2002.0031

Derdour, S., Ghenim, A.N., Megnounif, A., Tangang, F., Chung, J.X., Ayoub, A.B., 2022. Bias correction and evaluation of precipitation data from the CORDEX regional climate model for monitoring climate change in the Wadi Chemora Basin (Northeastern Algeria). Atmosphere, 13, 11, 1876. https://doi.org/10.3390/atmos13111876

Diedhiou, C.W., Panthou, G., Diatta, S., Sané, Y., Vischel, T., Camara, M., 2024. Simple scaling of extreme precipitation regime in Senegal. Sci. Afr., 23, e02034, https://doi.org/10.1016/j.sciaf.2023.e02034

Dobor, L., Hlásny, T., 2019. Choice of reference climate conditions matters in impact studies: Case of bias-corrected CORDEX data set. Int. J. Climatol., 39, 4, 2022–2040. https://doi.org/10.1002/joc.5930

Cheng, L., AghaKouchak, A., 2014. Nonstationary precipitation intensity-duration-frequency curves for infrastructure design in a changing climate. Sci. Rep., 4, 1, 1–6. https://doi.org/10.1038/srep07093

Chen, J., Yang, Y., Tang, J., 2022. Bias correction of surface air temperature and precipitation in CORDEX East Asia simulation: What should we do when applying bias correction? Atmos. Res., 280, 106439. https://doi.org/10.1016/j.atmosres.2022.106439

Feitoza Silva, D., Simonovic, S.P., Schardong, A., Avruch Goldenfum, J., 2021. Introducing non-stationarity into the development of intensity-duration-frequency curves under a changing climate. Water, 13, 8, 1008. https://doi.org/10.3390/w13081008

Földes, G., Labat, M.M., Kohnová, S., Hlavčová, K., 2022. Impact of changes in short-term rainfall on design floods: Case study of the Hnilec River Basin, Slovakia. Slovak Journal of Civil Engineering, 30, 1, 68–74. https://doi.org/10.2478/sjce-2022-0008

Friedlingstein, P., Jones, M. W., O'Sullivan, M., Andrew, R. M., Bakker, D. C., Hauck, J. et al., 2022. Global carbon budget 2021. Earth Sys. Sci. Data, 14, 4, 1917–2005. https://doi.org/10.5194/essd-14-1917-2022

Gampe, D., Schmid, J., Ludwig, R., 2019. Impact of reference dataset selection on RCM evaluation, bias correction, and resulting climate change signals of precipitation. J. Hydrometeorol., 20, 9, 1813–1828. https://doi.org/10.1175/JHM-D-18-0108.1

Ganguli, P., Coulibaly, P., 2017. Does nonstationarity in rainfall require nonstationary intensity–duration–frequency curves? Hydrol. Earth Sys. Sci., 21, 12, 6461–6483. https://doi.org/10.5194/hess-21-6461-2017

Ganguli, P., Coulibaly, P., 2019. Assessment of future changes in intensity-duration-frequency curves for Southern Ontario using North American (NA)-CORDEX models with nonstationary methods. J. Hydrol.: Reg. Stud., 22, 100587. https://doi.org/10.1016/j.ejrh.2018.12.007

Ghimire, U., Srinivasan, G., Agarwal, A., 2019. Assessment of rainfall bias correction techniques for improved hydrological simulation. Int. J. Climatol., 39, 4, 2386–2399. https://doi.org/10.1002/joc.5959

Gupta, V.K., Waymire, E., 1990. Multiscaling properties of spatial rainfall and river flow distributions. J. Geophys. Res.: Atmospheres, 95(D3), 1999–2009. https://doi.org/10.1029/JD095iD03p01999

Hempel, S., Frieler, K., Warszawski, L., Schewe, J., Piontek, F., 2013. A trend-preserving bias correction – the ISI-MIP approach. Earth Sys. Dyn., 4, 2, 219–236. https://doi.org/10.5194/esd-4-219-2013

Haerter, J.O., Hagemann, S., Moseley, C., Piani, C., 2011. Climate model bias correction and the role of timescales. Hydrol. Earth Sys. Sci., 15, 3, 1065–1079. https://doi.org/10.5194/hess-15-1065-2011

Hlavčová, K., Lapin, M., Valent, P., Szolgay, J., Kohnová, S., Rončák, P., 2015. Estimation of the impact of climate change-induced extreme precipitation events on floods. Contrib. Geophys. Geod., 45, 3, 173–192. https://doi.org/10.1515/congeo-2015-0019

Holthuijzen, M., Beckage, B., Clemins, P.J., Higdon, D., Winter, J.M., 2022. Robust bias-correction of precipitation extremes using a novel hybrid empirical quantile-mapping method:

Advantages of a linear correction for extremes. Theor. Appl. Climatol., 149, 1, 863–882. https://doi.org/10.1007/s00704-022-04035-2

Hosseinzadehtalaei, P., Tabari, H., Willems, P., 2018. Precipitation intensity–duration–frequency curves for central Belgium with an ensemble of EURO-CORDEX simulations, and associated uncertainties. Atmos. Res., 200, 1–12. https://doi.org/10.1016/j.atmosres.2017.09.015

Hui, Y., Xu, Y., Chen, J., Xu, C.Y., Chen, H., 2020. Impacts of bias nonstationarity of climate model outputs on hydrological simulations. Hydrol. Res., 51, 5, 925–941. https://doi.org/10.2166/nh.2020.254

Ivanov, M.A., Kotlarski, S., 2017. Assessing distribution-based climate model bias correction methods over an alpine domain: added value and limitations. Int. J. Climatol., 37, 5, 2633–2653. https://doi.org/10.1002/joc.4870

Johnson, F., Sharma, A., 2012. A nesting model for bias correction of variability at multiple time scales in general circulation model precipitation simulations. Water Resour. Res., 48, 1. https://doi.org/10.1029/2011WR010464

Katz, R.W., Parlange, M.B., Naveau, P., 2002. Statistics of extremes in hydrology. Adv. Water Resour., 25, 8-12, 1287–1304. https://doi.org/10.1016/S0309-1708(02)00056-8

Koutsoyiannis, D., Foufoula-Georgiou, E., 1993. A scaling model of a storm hyetograph. Water Resour. Res., 29, 7, 2345–2361. https://doi.org/10.1029/93WR00395

Koutsoyiannis, D., Kozonis, D., Manetas, A., 1998. A mathematical framework for studying rainfall intensity-duration-frequency relationships, J. Hydrol., 206, 1–2, 118–135. https://doi.org/10.1016/S0022-1694(98)00097-3

Koutsoyiannis, D., Iliopoulou, T., 2022. Ombrian curves advanced to stochastic modeling of rainfall intensity. In: Morbidelli, R. (Ed.): Rainfall - Modeling, Measurement and Applications. Elsevier, pp. 261–284. https://doi.org/10.1016/B978-0-12-822544-8.00003-2

Lehner, F., Nadeem, I., Formayer, H., 2020. An improved statistical bias correction method that also corrects dry climate models. Hydrol. Earth Sys. Sci. Discuss., 1–23. https://doi.org/10.5194/hess-2020-515

Lehner, F., Nadeem, I., Formayer, H., 2023. Evaluating skills and issues of quantile-based bias adjustment for climate change scenarios. Adv. Stat. Climatol., Meteorol. and Oceanogr., 9, 1, 29–44. https://doi.org/10.5194/ascmo-9-29-2023

Lenderink, G., Barbero, R., Loriaux, J.M., Fowler, H.J., 2017. Super-Clausius–Clapeyron scaling of extreme hourly convective precipitation and its relation to large-scale atmospheric conditions. J. Climate, 30, 15, 6037–6052. https://doi.org/10.1175/JCLI-D-16-0808.1

Lin, R., Zhu, J., Zheng, F., 2019. The application of the SVD method to reduce coupled model biases in seasonal predictions of rainfall. J. Geophys. Res.: Atmospheres, 124, 22, 11837–11849. https://doi.org/10.1029/2018JD029927

Mazzoglio, P., Butera, I., Alvioli, M., Claps, P., 2022. The role of morphology in the spatial distribution of short-duration rainfall extremes in Italy. Hydrol. Earth Sys. Sci., 26, 6, 1659–1672. https://doi.org/10.5194/hess-26-1659-2022

Mehrotra, R., Sharma, A., 2012. An improved standardization procedure to remove systematic low frequency variability biases in GCM simulations. Water Resour. Res., 48, 12. https://doi.org/10.1029/2012WR012446

Mehrotra, R., Sharma, A., 2019. A resampling approach for correcting systematic spatiotemporal biases for multiple variables in a changing climate. Water Resour. Res., 55, 1, 754–770. https://doi.org/10.1029/2018WR023270

Meitner, J., Štěpánek, P., Skalák, P., Dubrovský, M., Lhotka, O., Penčevová, R., Zahradníček, P., Farda, A., Trnka, M., 2023. Validation and selection of a representative subset from the ensemble of EURO-CORDEX EUR11 regional climate model outputs for the Czech Republic. Atmosphere, 14, 9, 1442. https://doi.org/10.3390/atmos14091442

Menabde, M., Seed, A., Pegram, G., 1999. A simple scaling model for extreme rainfall. Water Resour. Res., 35, 1, 335–339. https://doi.org/10.1029/1998WR900012

Mészáros, J., Halaj, M., Polčák, N., Onderka, M., 2022. Mean annual totals of precipitation during the period 1991–2015 with respect to cyclonic situations in Slovakia. Időjárás/Quarterly Journal of the Hungarian Meteorological Service, 126, 2, 267–284. https://doi.org/10.28974/idojaras.2022.2.6

Miao, C., Ashouri, H., Hsu, K.L., Sorooshian, S., Duan, Q., 2015. Evaluation of the PERSIANN-CDR daily rainfall estimates in capturing the behavior of extreme precipitation events over China. J. Hydrometeorol., 16, 3, 1387–1396. https://doi.org/10.1175/JHM-D-14-0174.1

Molnar, P., Burlando, P., 2005. Preservation of rainfall properties in stochastic disaggregation by a simple random cascade model. Atmos. Res., 77, 1–4, 137–151. https://doi.org/10.1016/j.atmosres.2004.10.024

National Weather Service, 2022. Analysis of Impact of Nonstationary Climate on NOAA Atlas 14 Estimates: Assessment Report. Available at: https://hdsc.nws.noaa.gov/hdsc/files25/NA14_Assessment_report_202201v1.pdf Accessed 05 May. 2024.

Ngai, S.T., Juneng, L., Tangang, F., Chung, J.X., Supari, S., Salimun, E. et al., 2022. Projected mean and extreme precipitation based on bias-corrected simulation outputs of CORDEX Southeast Asia. Weather Clim. Extremes, 37, 100484. https://doi.org/10.1016/j.wace.2022.100484

Nguyen, H., Mehrotra, R., Sharma, A., 2016. Correcting for systematic biases in GCM simulations in the frequency domain. J. Hydrol., 538, 117–126. https://doi.org/10.1016/j.jhydrol.2016.04.018

Nhat, L.M., Tachikawa Y., Sayama T., Takara K., 2007. Regional rainfall intensity duration frequency relationships for ungauged catchments based on scaling properties. Annuals of Disas. Prev. Res. Inst., Kyoto Univ., 50 B, 33–43. Available at: https://hywr.kuciv.kyoto-u.ac.jp/publications/papers/2007DPRI_Nhat.pdf Accessed 15 Apr. 2024.

Onderka, M., Pecho, J., 2021. Sensitivity of selected summertime rainfall characteristics to pre-event atmospheric and near-surface conditions. Atmos. Res., 259, 105671. https://doi.org/10.1016/j.atmosres.2021.105671

Onderka, M., Pecho, J., Bodinger, L., Bičárová, S., Lukasová, V., Buchholcerová, A., Nejedlík, P., 2022. Relationships between intensity, duration and frequency of short-term rains determined by Bayesian inference of GEV distribution parameters. Meteorogické zprávy /Meteorol. Rep., 75, 3, 81–88. (In Slovak.)

Onderka, M., Sokáč, M., Mikulová, K., Pecho, J., 2023. Digital atlas of rainfall design intensities in Slovakia. Meteorologický Časopis/Meteorol. J., 26, 1, 27–38. https://www.shmu.sk/File/met_cas/RR/2023-1_3%20Onderka.pdf Accessed 15 Apr. 2024.

Osuch, M., Romanowicz, R.J., Lawrence, D., Wong, W.K., 2016. Trends in projections of standardized precipitation indices in a future climate in Poland. Hydrol. Earth Sys. Sci., 20, 5, 1947–1969. https://doi.org/10.5194/hess-20-1947-2016

Piani, C., Haerter, J.O., Coppola, E., 2010. Statistical bias correction for daily precipitation in regional climate models over Europe. Theor. Appl. Climatol. 99, 187–192. https://doi.org/10.1007/s00704-009-0134-9

Poschlod, B., Ludwig, R., Sillmann, J., 2021. Ten-year return levels of sub-daily extreme precipitation over Europe. Earth Sys. Sci. Data, 13, 3, 983–1003. https://doi.org/10.5194/essd-13-983-2021

Ragno, E., AghaKouchak, A., Cheng, L., Sadegh, M., 2019. A generalized framework for process-informed nonstationary extreme value analysis. Adv. Water Resour., 130, 270–282. https://doi.org/10.1016/j.advwatres.2019.06.007

Rosso, R., Burlando, P., 1990. Scale invariance in temporal and spatial rainfall. In: Proceedings of XV General Assembly European Geophysical Society, Annales Geophysicae, 145, 23–27 April 1990, Copenhagen, Denmark.

Šamaj, F., 1959. Daily patterns of precipitation in the Danubian lowland and in the Tatra region. Acta Facultatis Rerum Naturalium Universitatis Comenianae, Meteorologia, 161–194. (In Slovak.)

Shaw, S.B., Royem, A.A., Riha, S.J., 2011. The relationship between extreme hourly precipitation and surface temperature in different hydroclimatic regions of the United States. J. Hydrometeorol., 12, 2, 319–325. https://doi.org/10.1175/2011JHM1364.1

Shin, J.Y., Lee, T., Park, T., Kim, S., 2019. Bias correction of RCM outputs using mixture distributions under multiple extreme weather influences. Theor. Appl. Climatol., 137, 201–216. https://doi.org/10.1007/s00704-018-2585-3

Schmith, T., Thejll, P., Berg, P., Boberg, F., Christensen, O.B., Christiansen, B., Christensen, J.H., Madsen, M.S., Steger, C., 2021. Identifying robust bias adjustment methods for European extreme precipitation in a multi-model pseudo-reality setting. Hydrol. Earth Sys. Sci., 25, 1, 273–290. https://doi.org/10.5194/hess-25-273-2021

Schroeer, K., Kirchengast, G., 2018. Sensitivity of extreme precipitation to temperature: the variability of scaling factors from a regional to local perspective. Clim. Dynam., 50, 3981–3994. https://doi.org/10.1007/s00382-017-3857-9

Schwalm, C.R., Glendon, S., Duffy, P.B., 2020. RCP8.5 tracks cumulative CO_2 emissions. Proceedings of the National Academy of Sciences, 117, 33, 19656–19657. https://doi.org/10.1073/pnas.2007117117

Singh, V.P., 2016. Handbook of Applied Hydrology, 2nd Ed. McGraw-Hill Education, New York, USA, 1440 p.

Szabó-Takács, B., Farda, A., Skalák, P., Meitner, J., 2019. Influence of bias correction methods on simulated Köppen−Geiger climate zones in Europe. Clim., 7, 2, 18. https://doi.org/10.3390/cli7020018

Szolgay J., Miklánek J., Výleta R., 2023. Interactions of natural and anthropogenic drivers and hydrological processes on local and regional scales: A review of main results of Slovak hydrology from 2019 to 2022. Acta Hydrologica Slovaca, 24, 2, 254–265. https://doi.org/10.31577/ahs-2023-0024.02.0028

Teutschbein, C., Seibert, J., 2013. Is bias correction of regional climate model (RCM) simulations possible for non-stationary conditions? Hydrol. Earth Sys. Sci., 17, 12, 5061–5077. https://doi.org/10.5194/hess-17-5061-2013

Tootoonchi, F., Todorović, A., Grabs, T., Teutschbein, C., 2023. Uni-and multivariate bias adjustment of climate model simulations in Nordic catchments: Effects on hydrological signatures relevant for water resources management in a changing climate. J. Hydrol., 623, 129807. https://doi.org/10.1016/j.jhydrol.2023.129807

Vyshnevskyi, V., Shevchuk, S., 2022. Impact of climate change and human factors on the water regime of the Danube Delta. Acta Hydrologica Slovaca, 23, 2, 207–216. https://doi.org/10.31577/ahs-2022-0023.02.0023

Wasko, C., Sharma, A., 2015. Steeper temporal distribution of rain intensity at higher temperatures within Australian storms. Nat. Geosci., 8, 7, 527–9. https://doi.org/10.1038/ngeo2456

Wasko, C., Sharma, A., 2017. Continuous rainfall generation for a warmer climate using observed temperature sensitivities. J. Hydrol., 544, 575–90. https://doi.org/10.1016/j.jhydrol.2016.12.002

Wood, A.W., Leung, L.R., Sridhar, V., Lettenmaier, D.P., 2004. Hydrologic implications of dynamical and statistical approaches to downscaling climate model outputs. Clim. Change, 62, 1, 189–216. https://doi.org/10.1023/B:CLIM.0000013685.99609.9e

Yu, P.S., Yang, T.C., Lin, C.S., 2004. Regional rainfall intensity formulas based on scaling property of rainfall. J. Hydrol., 295, 1–4, 108–123. https://doi.org/10.1016/j.jhydrol.2004.03.003

Zhao, W., Kinouchi, T., Nguyen, H.Q., 2021. A framework for projecting future intensity-duration-frequency (IDF) curves based on CORDEX Southeast Asia multi-model simulations: An application for two cities in Southern Vietnam. J. Hydrol., 598, 126461. https://doi.org/10.1016/j.jhydrol.2021.126461

Received 1 august 2024
Accepted 10 October 2024